Available online at www.sciencedirect.com
ScienceDirect
Biochimica et Biophysica Acta 1773 (2007) 1546–1557
Biochimica et Biophysica Acta BBA
www.elsevier.com/locate/bbamcr

Cystein cathepsin and Hsp90 activities determine the balance between apoptotic and necrotic cell death pathways in caspase-compromised U937 cells

Gergely Imre [a], Zsuzsanna Dunai [a], Istvan Petak [a,b], Rudolf Mihalik [a,b,*]

[a] *Department of I.st Pathology and Experimental Cancer Research, Semmelweis University, Budapest, 1085, Hungary*
[b] *Rational Drug Design Laboratories, Cooperative Research Center, Semmelweis University, Budapest, 1113 Hungary*

Received 20 February 2007; received in revised form 25 June 2007; accepted 12 July 2007
Available online 19 July 2007

Abstract

Caspase-inhibited cells induced to die may exhibit the traits of either apoptosis or necrosis or both, simultaneously. However, mechanisms regulating the commitment to these distinct forms of cell death are barely identified. We found that staurosporine induced both apoptotic and necrotic traits in U937 cells exposed to the caspase inhibitor benzyloxycarbonyl-Val-Ala-DL-Asp(OMe)-fluoromethylketone. Morphology and flow cytometry revealed that individual cells exhibited either apoptotic or necrotic traits, but not the mixed phenotype. Inhibition of cathepsin activity by benzyloxycarbonyl-Phe-Ala-fluoromethylketone rendered caspase-compromised cells resistant to staurosporine-induced apoptosis, but switched the cell death form to necrosis. Inhibition of heat shock protein 90 kDa (Hsp90) chaperon activity by geldanamycin conferred resistance to necrosis in caspase-compromised cells but switched the cell death form to apoptosis. Combination of benzyloxycarbonyl-Phe-Ala-fluoromethylketone and geldanamycin halted the onset of both forms of cell death by saving mitochondrial trans-membrane potential and preventing acidic volume (lysosomes) loss. These effects of benzyloxycarbonyl-Phe-Ala-fluoromethylketone and/or geldanamycin on cell death were restricted to caspase-inhibited cells exposed to staurosporine but influenced neither only the staurosporine-provoked apoptosis nor hydrogen peroxide (H_2O_2)-generated necrosis. Our results demonstrate that the staurosporine-induced death pathway bifurcates in caspase-compromised cells and commitment to apoptotic or necrotic phenotypes depends on cathepsin protease or Hsp90 chaperon activities.

Keywords: Apoptosis; Caspase-independent; Cathepsin; Heat shock protein 90 kDa; Necrosis; Staurosporine

1. Introduction

It is accepted that the main, but not obligate, hallmark of apoptosis is the activation of caspases resulting in cleavage of a selective pool of proteins, loss of phospholipid assymetry in the plasma membrane and early oligonucleosomal DNA fragmentation. These events are accompanied by characteristic morphological changes of the cell, such as shrinkage and condensation. On the contrary, necrosis is marked by oncosis and dilution in the morphological appearance, accompanied by early loss of the integrity of plasma membrane and intracellular compartments. Usually these traits of apoptosis and necrosis appear in separate cells, but sometimes they may appear combined in individual cells as atypical forms of cell death [11,25,55,60].

When caspase activity is suppressed in cells (e.g. in the presence of caspase inhibitor), an apoptosis-prone stimuli (especially

Abbreviations: AIF, apoptosis inducing factor; AO, acridine orange; $DiOC_6$ (3), 3,3′-Dihexyiloxacarbocyanine iodide; FL, fluorescence; FSC, forward light scatter; GA, geldanamycin; Hsp90, heat shock protein 90 kDa; PARP, poly (ADP-rybose) polymerase; PI, propidium iodide; RIP1, receptor-interacting protein 1; SSC, side light scatter; STS, staurosporine; TNF, tumor necrosis factor; z-DEVD-amc, benzyloxycarbonyl-Asp(OMe)-Glu(OMe)-Val-DL-ASP (OMe)-7 aminomethylcoumarin; z-FA.fmk, benzyloxycarbonyl-Phe-Ala-fluoromethylketone; z-FR.amc, benzyloxycarbonyl-Phe-Arg-aminomethylcoumarin; z-RR.amc, benzyloxycarbonyl-Arg-Arg-aminomethylcoumarin; z-VAD.fmk, benzyloxycarbonyl-Val-Ala-Asp(OMe)-fluoromethylketone

* Corresponding author. Department of I.st Pathology and Experimental Cancer Research, Semmelweis University, Budapest, 1085, Hungary. Tel.: +36 1 459 1500; fax: +36 1 317 1074.
E-mail address: mihalik@korb1.sote.hu (R. Mihalik).

0167-4889/$ - see front matter © 2007 Elsevier B.V. All rights reserved.
doi:10.1016/j.bbamcr.2007.07.003

known in the case of TNF-α) may induce apoptotic(-like) or necrotic(-like) cell death forms depending on the cell type [18,26,57]. The mechanisms regulating the commitment to these distinct cell death forms are studied mainly in death receptor models, with the use of caspase inhibitors or genetically modified cells but barely explored with other type of cell death inducers [12,21,31–33,38,56].

Staurosporine (STS) – a poorly selective inhibitor of protein kinases – is a widely applied model compound for inducing cell death [50]. Treatment with STS induces the mitochondrial pathway of apoptosis, activates the Bax protein [64] and promotes its translocation to the mitochondria [48]. Consequently, the outer membrane of the mitochondria becomes permeabilized, allowing the release of proapoptotic proteins such as cytochrome *c*, Omi/HtrA2 and AIF [8,43,45,49,58]. Cytochrome *c* initiates apoptosome formation, activation of caspase-9 and the executioner caspases (-3, -6, -7). Caspases process their selective target proteins, thereby evoking the maturation of the apoptotic morphology [65].

Recent results, however, revealed that STS could induce regulated cell death even in the presence of caspase inhibitors. The mechanism and the morphological appearance of this cell death were differently defined in the various cell models. In caspase-compromised cells, STS could induce neither the proteolytic processing of caspase target proteins nor the large scale DNA fragmentation, but initiated prominent chromatin condensation [2,12]. However, the STS-induced cell death forms were distinct in various caspase-compromised models. In some cases, apoptotic (-like) [4,9,14,15,62] and in other cases, necrotic (-like) [1,63] cell death forms were concluded to be dominant.

Previously, we have reported that CA-074Me abrogated STS-induced cell death (both apoptotic and necrotic) in caspase-inhibited leukemia cells independently from the inhibitory effect of CA-074Me on cathepsin B [36]. This study was designed to reveal how individual caspase-inhibited U937 cells committed to apoptosis or to necrosis or maybe simultaneously to a mixed phenotype when exposed to STS and what role cystein cathepsins other than cathepsin B play in these processes.

2. Materials and methods

2.1. Materials

z-Val-Ala-Asp(OMe)-fluoromethylketone (z-VAD.fmk) and Z-Phe-Ala-FMK (z-FA.fmk) were purchased from both Enzyme System Product (MP Biomedicals, Solon, OH USA) and Bachem (Bubendorf, Switzerland). z-DEVD-amc, z-RR-amc, z-FR-amc were from Bachem. Staurosporine and geldanamycin were from Sigma (St. Louis, MO, USA).

2.2. Cell culture

U937 promonocytic cell line was cultured in RPMI 1640 (Sigma) with 10% heat inactivated fetal bovine serum (Sigma), 2 mM L-glutamine and 100 μg/mL penicillin–streptomycin (Sigma) at 5% CO_2 and 37 °C in a humidified chamber. Cells were regularly tested for the expression of some human CD antigens: CD45 (+); CD33(+); CD13(+); CD34(−); CD14(−); CD4(−). Antibodies were directly labeled with fluorochrome and purchased from Becton-Dickinson (Franklin Lakes, NJ, USA). For treatment, cells were plated in 0.5 mL onto 48-well suspension plate (Greiner) at 3×10^5 cells/mL as control and 5×10^5 cells/mL for geldanamycin (GA; 1 μM) pretreatment for 12 h as geldanamycin inhibited cell proliferation. Then cells were exposed to z-FA.fmk (z-FA; 1 μM) and/or z-VAD (OMe).fmk (z-VAD.fmk; 50 μM) 30 min before staurosporine (STS; 1 μM). Cells were incubated with STS for 8 h.

2.3. Detection of cell death associated functional changes by flow cytometry

The samples were detected with FACScalibur or FACScan flow cytometers (Becton Dickinson). Data were analyzed with WINLIST software (VERITY Software House, Topsham, USA). The following standard light filters were applied to fluorescence channels: FL1: 530/30 nm; FL2: 585/42 nm; FL3: 650LP. Analysis was performed on the amplitude (height, H) of the fluorescence signal in log scale. Doublet discrimination panel was set on FL2 channel for detection of FL2A (area) and FL2W (width) characteristics of the fluorescence signal in linear scale. The terms of various flow cytometric representations used in the following paragraphs include sample preparation, the profile of flow cytometric detection, gating strategy and data analysis.

2.4. [PI uptake] representation of plasma membrane damage

Treated cells were stained with 0.5 mL PBS containing 5 mM glucose and 10 μg/mL propidium iodide (PI) (Sigma) in the plate, and incubated for 15 min on 37 °C before measurement. Necrotic (PI+) cells usually lost light scatter intensity therefore they mixed up with debris in the [FSC, SSC] two-dimensional parameter diagram. For gating necrotic cells out of debris we applied [FSC, FL3H] diagram where necrotic cells contained high amount of DNA could be separated from debris contained low amount of DNA. Gated cells were analyzed on FL2H log scale histograms and data were presented as percentage of cells in the marked region of the histogram (Fig. 2D). Alternatively, samples stained with $DiOC_6(3)$ or annexin V-FITC together with PI was also exploited for analysis in [PI uptake] representation.

2.5. [Annexin V-FITC, PI] representation of phosphatidylserine distribution in the plasma-membrane

The assay was performed according to the suggestions of the vendor (Alexis Biochemicals, Lausen, Switzerland). Treated cells were stained with 0.5 mL PBS containing 5 mM glucose and 10 μg/mL PI in the plate and incubated for 10 min on 37 °C. After centrifugation (300×*g*/2 min), the cells were suspended in 400 μL binding buffer (10 mM HEPES, 140 mM NaCl, 2.5 mM $CaCl_2$). 80 μL of the sample in binding buffer was mixed with 20 μL annexin V-FITC solution (5 μL annexinV-FITC was dissolved in 15 μL binding buffer). After 10 min incubation in the dark additional 400 μL of binding buffer (containing 1 μg/mL PI) was added to the samples and measured immediately. The [FSC, FL3H] diagram was applied for gating and the gated cells were analyzed in [FL1H, FL2H] log scale two-dimensional diagram. Auto-fluorescence of the cells was positioned in first decade, and compensation for FITC fluorescence in the FL2 channel was applied. Data were presented as percentage of cells in the marked regions of the diagram (Fig. 4A).

2.6. [$DiOC_6(3)$] representation of the mitochondrial trans-membrane potential

Samples were prepared according to Darzynkiewicz and Bender [10], with modifications. Treated cells were stained with 0.5 mL PBS containing 5 mM glucose, 10 nM $DiOC_6(3)$ (Sigma) and 10 μg/mL PI in the plate and incubated for 15 min on 37 C° before harvesting and measurement without washing. Cells were gated in [FSC, FL3H] diagram, analyzed on FL1H log scale histograms and the data were presented as mean fluorescence intensity of the whole gated cell population (Fig. 7A, B).

2.7. [AO red] representation of the volume of acidic compartments

Samples were prepared according to Traganos and Darzynkiewicz [54], with modifications. Acridine orange (AO) is a metachrome dye providing green fluorescence at low concentration (e.g. when intercalated into ds-DNA) and red fluorescence at high concentration (e.g. when amassed in the acidic

compartments of the living cell). Treated cells were stained with 0.5 mL PBS containing 5 mM glucose and 5 μg/mL AO (Sigma) in the plate and incubated for 15 min on 37 C°. After centrifugation (300×*g*/2 min) the cells were suspended in 1 mL PBS containing 5 mM glucose and measured immediately. Cells were gated in [FL1H, FL3H] diagram for discriminating cells with high DNA content from debris with low amount of DNA. The gated populations were analyzed on FL3H log scale histograms and the data were presented as mean fluorescence intensity of the whole population (Fig. 7E, F).

2.8. [Sub-G1] representation of oligonucleosomal DNA fragmentation

Samples were prepared according to Gong et al. [22]. Treated cells were centrifuged (300×*g*/2 min) and the pellets were suspended in 1 mL 70% ethanol (−20 °C), let the cells fixed on room temperature for 30 min and stored on −20 °C. Oligonucleosomal DNA fragments were extracted from ethanol-fixed cells in 750 μL extraction buffer containing 200 mM Na_2HPO_4/citric acid (pH=7.8) and 10 μg/mL RNAse A (Sigma) for 15 min, then stained with PI (propidium iodide, 5 μg/mL for final concentration) for at least 10 min before measurement. Cells were gated in (FSC, FL2H) diagram for discriminating debris and analyzed on FL2H log scale histogram as percentage of cells in the marked, sub-G1 region.

2.9. [SSC, DNA content] representation of light scatter change and DNA fragmentation

Cells were fixed, stained and gated according to the [sub-G1] representation. The gated populations were analyzed on the (SSC, FL2H) diagrams marked regions as (SSC^{norm}, DNA^{low}) for apoptotic cells, (SSC^{low}, DNA^{norm}) for necrotic cells and (SSC^{low}, DNA^{low}) for cells with a mixed, atypical phenotype and percentage of cells in this regions were presented (Fig. 2D).

2.10. Cell cycle analysis

Cells were fixed and stained according to [sub-G1] representation. Cells were gated in (FSC, FL2H) diagram in combination with (FL2A, FL2W) diagram for inclusion of sub-G1 dead cells and exclusion of doublets. The gated population was analyzed on FL2A linear scale histogram, markers were set on the border of G1-S and on the first quarter of S cell cycle phase and percentage of the cell in this region was presented.

2.11. Cleaved PARP western blot analysis

0.5×10^6 cells were treated with drugs as described above. At the end of the incubation cells were washed in PBS and pelleted (100 g, 4 min). The pellet was resuspended in 50 μL 2× Laemmli buffer (62.5 mM Tris–HCl, pH 6.8, 2% SDS, 25% glycerol, 0.01% Bromophenol Blue) with 5% mercaptoethanol. Each samples was boiled for 3 min. Electrophoresis was performed in a 10% polyacrylamide gel. Rabbit polyclonal antibody against PARP (#9542, Cell Signaling Technology; Kvalitex, Budapest, Hungary) was used to detect full length PARP (116 kDa) and cleaved fragment (89 kDa). Horseradish peroxidase-conjugated goat anti-rabbit IgG (#7074, Cell Signaling Technology) was employed as secondary antibody. Detection was performed using ECL western blotting substrate (#32106, PIERCE). Visualization was done by Kodak Image Station 4000 MM and Kodak Molecular Imaging Software 4.0.3 was used to determine the density of the bands. The density of the fragment was expressed as percentage of the sum of the density of the fragment and the full length PARP bands.

2.12. Protease activity assays

The treated cells (0.5×10^6 cells/mL) were incubated for different time points and then washed in PBS two times (300 g/2 min). Samples were suspended in 100 μL caspase buffer (50 mM HEPES (pH 7.4), 100 mM NaCl, 0.1% (w/v) CHAPS, 10% (w/v) sucrose, +10 mM DTT (freshly added)) or cathepsin buffer (Na_2HPO_4/NaH_2PO_4 pH6, 1 mM EDTA, 1 mM DTT (freshly added)). After transferring samples into 96-well plates Triton X-100 (0.2%) were added, and cell lysis was completed by repeated pipetting. Caspase substrate z-DEVD.amc (20 μM) or cathepsin substrates z-FR.amc (50 μM) or z-RR.amc (50 μM) were added, and fluorescence intensities of libareted AMC was recorded for 15 min by a fluorescence plate reader Fluoroskan Ascent (Thermo Fisher Scientific, Waltman MA, USA). Protease activity was determined from the slope of the AMC fluorescence. Activity was presented as percentage of control, vehicle-treated samples.

2.13. Agarose gel electrophoresis

The samples were dissolved in 100 microL/10^6 cells buffer solution containing: 100 mM EDTA, 10 mM TRIS (pH=8) 0.5% SDS (and proteinase K in 0.1 mg/mL concentration added freshly) at least 1 h at 50 °C. Then RNase (DNase free) were added to the samples in 0.2 mg/mL concentration and cells were kept on 30 °C overnight. The samples were run on 1% agarose gel and then were stained in ethidium bromide (for 15 min) and detected under UV light.

2.14. Light microscopic studies

Cytospin preparations were fixed in methanol, stained with hematoxylin–eosin, then were dehydrated with ethanol, acetone and xilol. The morphological changes of apoptosis were studied by light microscopy. 200 cells per slide were counted and the number of apoptotic and necrotic cells were determined. Cells were categorized according to Daugas et al. [12]: stage I, apoptotic cell condensed moderately (including smooth nuclei); stage II. apoptotic cells had full blown nuclear condensation (pyknosis) and formation of nuclear apoptotic bodies (karyorrhexis). Necrosis was characterized by cell swelling and blurred plasma membrane. Cells with washed out cytoplasm, the so-called ghosts, were identified as late necrotic cells.

2.15. Electron microscopy

Samples (0.5×10^6 cells) were spun (200×g/5 min) onto slide (slides were covered with parlodion and heated for better adhesion) then fixed in glutaraldehyde (2.5%, 30 min, 4 °C) and kept in PBS overnight at 4 °C. Next day the slides were incubated in OsO_4 (dissolved in PBS) for at least 90 min then washed in PBS (for 10 min). The samples were dehydrated in rising concentration of ethanol (50–75–96–100%), then EPON-812 (1:1 in abs. ethanol) was dropped to the samples for 1 h. Capsules containing EPON-812 were placed onto samples and were kept in 60 °C for a day to let the resin polymerized. Samples were separated from slides by cooling in liquid nitrogen. Thin sections were cut by LKB-Ultrotom-3A. The slices were placed on a grid. Samples were treated (2% uranil-acetat for 10 min, lead citrate for 2 min) to get contrast and then examined under transmission electron microscope (Philips, CM-10).

2.16. Statistics

All experiments were repeated at least twice. Significance was determined by Student's *t*-probe (two tailed, paired) using Microsoft Excel and the indicated significance on graphs are: $P<0.05$ (*); $P<0.01$ (**); $P<0.001$ (***).

3. Results

3.1. Staurosporine induced delayed apoptotic and necrotic cell death forms in caspase- compromised cells

We performed time-course experiments to determine the kinetic appearance of cell death features in U937 cells exposed to STS (1 μM) in the absence or presence of pan caspase inhibitor z-VAD.fmk (50 μM). STS alone induced caspase 3-like DEVDase activity after 2 h, accompanied by small scale DNA fragmentation detected by flow cytometry as sub-G1 cells (Fig. 1A). Plasma membrane damage occurred only several hours later, possibly as a sign of secondary necrosis (PI+ cells) detected by PI staining.

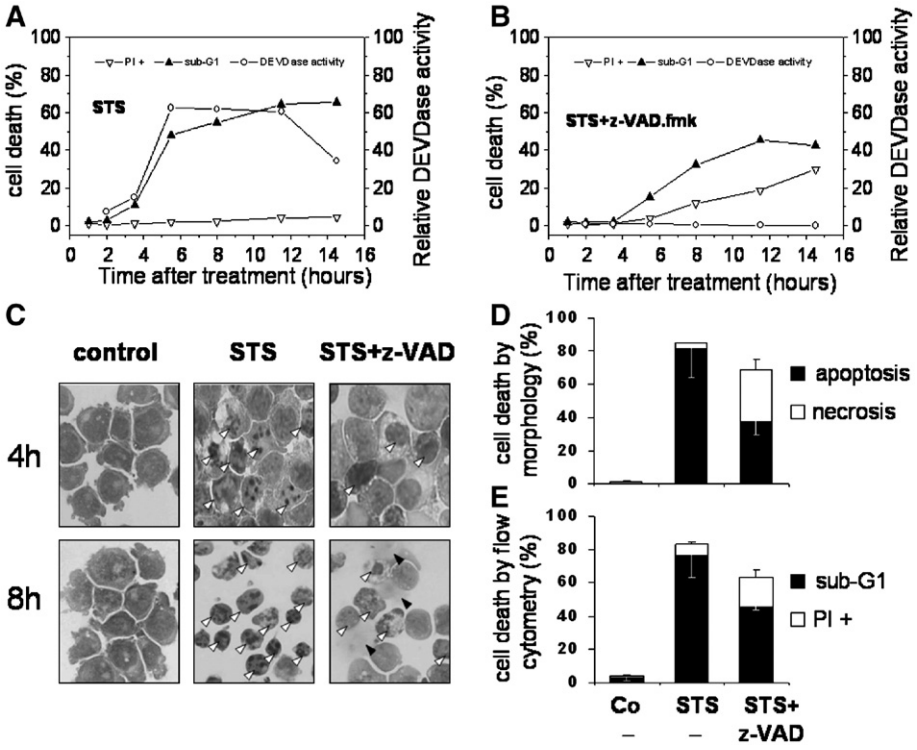

Fig. 1. Staurosporine-induced delayed apoptotic and necrotic cell death forms in caspase-compromised cells. U937 cells were exposed to STS (1 μM) in the presence or absence of z-VAD.fmk (z-VAD) (50 μM) or DMSO as vehicle. Time kinetics of cell death (sub-G1: cells with fragmented DNA; PI+: cells with plasma membrane damage) and effector caspase (DEVDase) activity (detected with z-DEVD.amc fluorogenic substrate) in samples exposed to (A) STS or (B) STS+z-VAD.fmk. ($n=2$). (C) Cells were treated as indicated and stained with hematoxylin–eosin. Arrows indicate apoptotic (white) or necrotic (black) cells. (D) Counting of apoptotic and necrotic cells based on morphological criteria ($n=2$) after 8 h treatments. (E) The same experiments evaluated in [sub-G1] and [PI uptake] flow cytometric death profiles.

In the presence of caspase inhibitor, STS did not evoke DEVDase activity for up to 15 h (Fig. 1B). However, we could detect a gradually increasing number of sub-G1 cells and PI-positive cells after 5 h of treatment, indicating the formation of apoptotic cells and necrotic cells in synchrony. Morphological investigation of hematoxylin–eosin-stained samples revealed that STS generated a great number of cells with stage II apoptotic nuclear morphology that included nuclear fragmentation (karyorrhexis) and condensation [12] (Fig. 1C). The ratio of cells with stage II apoptotic morphology was in good correlation with sub-G1 cells (Fig. 1D–E). At 4 h of treatment, z-VAD.fmk inhibited the STS-provoked manifestation of karyorrhexis but allowed (at least partially) the cell and nuclear condensation to proceed, the sign of stage I apoptosis (Fig. 1C). However, stage II cells appeared later at 8 h of treatment, frequently with dominant nuclear condensation on the periphery of the nuclei (Fig. 1C). The number of cells with nuclear condensation correlated well with the number of sub-G1 cells (Fig. 1D–E).

3.2. STS-induced apoptotic or necrotic phenotypes related to distinct caspase- compromised cells

Electron microscopy confirmed that STS+z-VAD.fmk-treated U937 cells became either apoptotic (A) (with a similar phenotype to STS exposed cells) or necrotic (N) with non-condensed, smooth chromatin without hetero-chromatin and cytoplasm without a resolved structure (Fig. 2A). In these cells, the nucleus double bilayer membrane was often split, the intermembrane space was dilated, and the cytoplasm was partially or entirely detached from the nucleus (black arrows, Fig. 2A).

Searching discriminative properties of cell death forms, we observed that unfixed, PI-positive necrotic cells showed not only the well-known loss of forward (light) scatter (FSC) property, but also considerable loss of side (light) scatter (SSC) property detected by flow cytometry, after STS treatment of caspase compromised cells (Fig. 2B). Interestingly, after ethanol fixation and processing of samples according to [sub-G1] representation, this population of cells reserved the properties of diminished SSC, while PI stained these cells with the same fluorescence intensity as non-dead (ND) (or untreated) cells with fully retained DNA content (SSC^{low}, DNA^{norm}) (Fig. 2B). The percentage of this (SSC^{low}, DNA^{norm}) population in fixed samples correlated well with the percentage of the PI-positive population in vitally PI-stained samples (Fig. 2C). The loss of the SSC property of necrotic caspase-compromised cells in flow cytometry was possibly related to the loss of the cytoplasm and/or the loss of heterochromatin observed with electron microscopy (Fig. 2A). In apoptotic cells, the normal SSC property was well preserved after ethanol fixation either in STS- or STS+z-VAD.fmk-exposed samples after 8 h of treatment (SSC^{norm}, DNA^{low}) (Fig. 2D). When cells were treated with STS for prolonged time (20 h), secondary necrosis ensued apoptosis (Fig. 2D). But post-apoptotic necrotic cells lost their SSC value only gradually and this was possibly

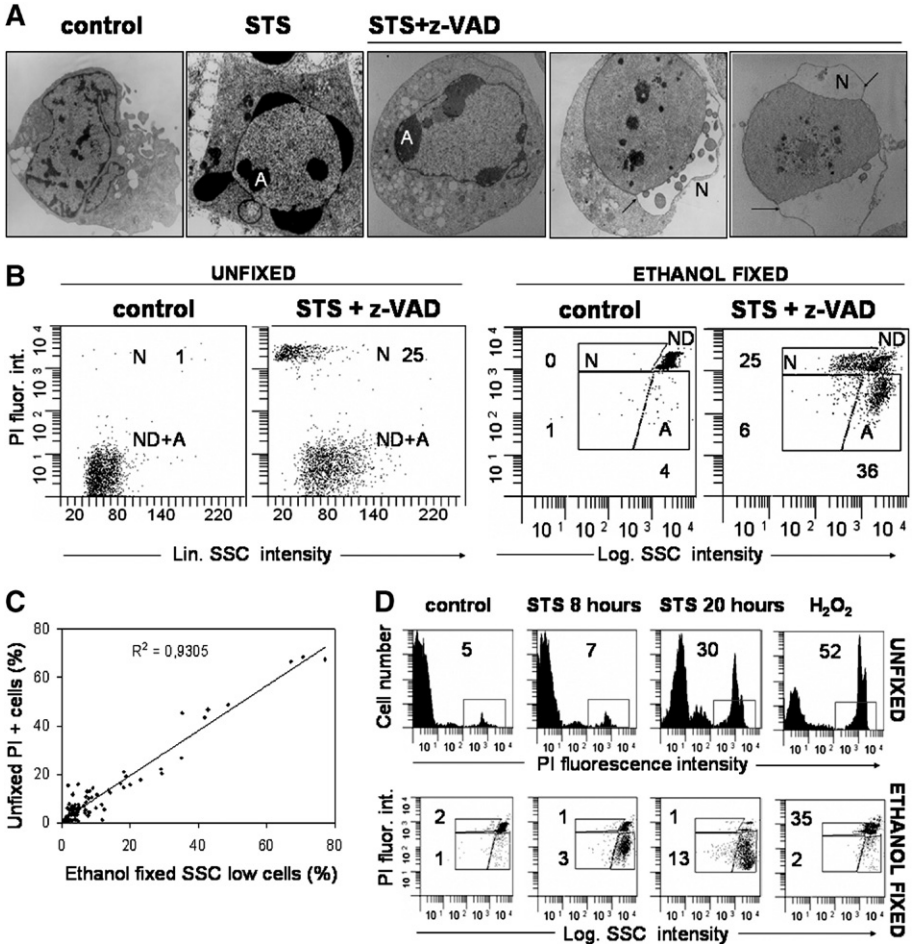

Fig. 2. STS-induced apoptotic or necrotic phenotypes related to distinct caspase-compromised cells. (A) U937 cells were exposed to STS (1 μM) in the presence or absence of z-VAD.fmk (50 μM) for 8 h. Samples were prepared for ultrastructural investigation. Black arrows indicate unstuck nucleus membrane. A: apoptotic, N: necrotic cell. (B) Cells were exposed to STS (1 μM) in the presence of z-VAD.fmk (50 μM) for 8 h and prepared for flow cytometry measurement. PI-stained UNFIXED samples were presented in FL2-SSC cytogram (SSC in linear scale). PI-stained ETHANOL FIXED cells evaluated in [SSC, DNA content] representation (SSC in logarithmic scale). Inserted values on representative histograms show the percentage of the marked population. A: apoptotic, N: necrotic, ND: not dead cells. (C) Correlation between absolute percentage of PI+ cells in unfixed samples and SSC low intensity cells in ethanol fixed samples. Points represent the various treatments indicated in Fig. 4C column diagrams. (D) Cells were exposed to STS (1 μM) for 8 or 20 h or H_2O_2 (2.5 mM) for 8 h and prepared for flow cytometry measurement. Histograms of PI-stained UNFIXED samples evaluated in [PI uptake] representation. Histograms of PI-stained ETHANOL FIXED cells evaluated in [SSC, DNA content] representation. Inserted values on representative histograms show the percentage of the marked population.

the sign of post-mortem degradation of DNA and the remains of cell structure. In the case of H_2O_2-provoked necrosis (2.5 mM, 8 h), a comparable ratio of cells lost their plasma membrane integrity and their SSC property. However, the lost SSC intensity was considerably less in necrotic cells exposed to H_2O_2 than in necrotic cells generated by STS+z-VAD.fmk. This difference may signify some variance in the activated necrotic pathways.

Our data indicate that the STS+z-VAD.fmk-induced cell death pathway bifurcates in individual cells and commitment to apoptosis is associated with high grade DNA fragmentation while primary necrosis is associated with considerable loss of SSC (in correlation with plasma membrane damage).

3.3. STS-induced cell death is associated with cystein cathepsin protease activity in caspase-compromised cells

To explore the mechanistic elements of cell death in caspase-compromised cells, we performed DNA gel electrophoresis and PARP cleavage western blot assays. The appearance of nucleosomal DNA ladder formation and PARP cleavage confirmed the apoptotic features of STS-induced cell death. Both DNA laddering and PARP processing were only partially reduced in the presence of z-VAD.fmk (Fig. 3A–B). Nucleosomal DNA fragmentation and the size of cleaved PARP, as well as the correlation of DNA fragmentation with PARP cleavage at variable concentrations of z-VAD.fmk (Fig. 3C), support the assumption of the presence of caspase-like protease activity in caspase-compromised cells, even when cell lysates were free of detectable DEVDase activity (Fig. 3C). To resolve this discrepancy, we looked for other protease activity in U937 cells that may be responsible for PARP cleavage. Though lysosomal cystein cathepsins reportedly have affinity for z-VAD.fmk (or its precursor form z-VAD(OMe).fmk) [42,44], we assessed the cathepsin (FRase and RRase) activity in cells treated with increasing concentrations of z-VAD.fmk. In comparison to fully eliminated DEVDase (Fig. 3C) or RRase (not shown) activity, a

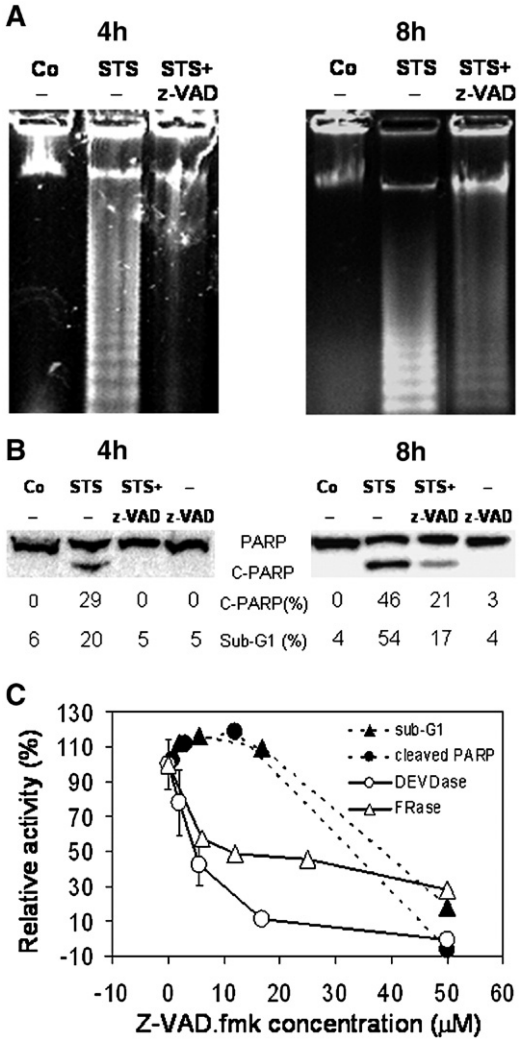

Fig. 3. Assessment of protease and DNase activities. (A, B) U937 cells were exposed to STS (1 μM) in the presence or absence of z-VAD.fmk (z-VAD) (50 μM) for 4 and 8 h. Samples were harvested for (A) DNA agarose gel electrophoresis, (B) western blot analysis and flow cytometric detection. PARP: full length PARP (116 kDa), C-PARP: cleaved PARP fragment (89 kDa). Values indicate percentage of C-PARP (western blot) and percentage of sub-G1 cells (Flow cytometry). (C) Cells were exposed to STS in combination with dilutions of z-VAD.fmk for 4 h. DEVDase (caspase) activity was detected by z-DEVD.amc fluorogenic substrate cleavage; FRase activity was detected by z-FR.amc fluorogenic substrate cleavage; sub-G1 cells were detected by flow cytometry; PARP fragmentation was analyzed by western blotting and the percentage of C-PARP was showed on the diagram.

residual fraction of around 40% of FRase activity remained in the lysates of cells exposed to >10 μM z-VAD.fmk (Fig. 3C), indicating the presence of z-VAD.fmk resistant cathepsin-like protease activity in U937 cells.

The involvement of cystein cathepsin proteases in STS+z-VAD.fmk-generated cell death was tested by z-FA.fmk, the broad spectrum inhibitor of cathepsins (B, L, H) [37]. In all three ([annexin V—PI], [sub-G1—PI uptake] and [SSC—DNA content]) of the flow cytometric cell death profiles, z-FA.fmk decreased the appropriate population of apoptotic cells ($p=0.0002$ in [sub-G1—PI uptake] profile) while increasing the necrotic population ($p=0.0051$ in [sub-G1—PI uptake] profile) in STS+zVAD.fmk-treated samples (Fig. 4A–C); however, z-FA.fmk was ineffective on STS-induced apoptosis (Fig. 4A–C) and H_2O_2-induced necrosis (not shown). The z-FA.fmk-augmented population of (SSC^{low}, DNA^{norm}) necrotic cells in [SSC—DNA content] profile shows the same decrease is SSC intensity indicating that excess necrotic cells may follow the same necrotic death pathway (Fig. 4B). Residual PARP cleavage in STS+z-VAD.fmk samples was eliminated by z-FA.fmk treatment, while it was not affected in STS-generated samples (Fig. 4D). Morphological signs of DNA condensation were also extinguished by z-FA.fmk visualised in H–E-stained preparations (Fig. 5A). Inhibition of apoptotic cell death and inhibition of cathepsin activity in cell lysates was well correlated over broad range of z-FA.fmk concentrations (Fig. 6A).

These results indicate that cystein cathepsin protease activity is required for the apoptotic death program induced by STS in caspase-compromised U937 cells.

3.4. STS-induced necrosis required Hsp90 chaperone activity in caspase-compromised cells

RIP1 (Receptor Interacting Protein 1) kinase is a central component of several necrotic signaling pathways [16] and RIP1 protein, being the client of the Hsp90 chaperone, is down-regulated by prolonged treatment with geldanamycin (GA) [26,56], an inhibitor of Hsp90 [46].

We pretreated U937 cells with GA for 12 h to ensure the down-regulation of Hsp90 client proteins. In all three ([annexin V—PI], [sub-G1—PI uptake] and [SSC—DNA content]) of the flow cytometric cell death profiles, GA decreased the appropriate population of necrotic cells ($p=0.0032$ in [sub-G1—PI uptake] profile), while increasing the apoptotic population in STS+zVAD.fmk-treated samples (Fig 4A–C), but did not change either STS-induced apoptotic (Fig. 4A–C) or H_2O_2-induced necrotic cell death (not shown). GA slightly augmented the cleavage of PARP in STS+z-VAD.fmk samples in concordance with an enlarged sub-G1 population (Fig. 4C, D) and increased the number of cells with stage II nuclear morphology (Fig. 5A, C). Inhibition of Hsp90 activity by GA is known to induce cell cycle arrest in G1 as well as in G2/M phases [3]. We assessed and found that the two functions of GA (modulation of the cell death and the cell cycle) were similarly affected by GA dilutions, confirming that both functions are related to inhibition of Hsp90 (Fig. 6B).

These results indicate that Hsp90 chaperone activity is required for the necrotic death program induced by STS in the caspase-compromised U937 cells.

3.5. GA and z-FA.fmk co-treatment rescued STS-induced caspase-compromised cells by reducing mitochondrial and lysosomal breakdown

So far, neither one of the two inhibitors (GA or z-FA.fmk) inhibited cell death when used alone—they only switched one of the cell death forms to the other. Next, we assessed if co-treatment could abrogate the STS+z-VAD.fmk-provoked cell death.

We found that all hallmarks of apoptosis (annexin V positivity and sub-G1 population) and necrosis (PI uptake and

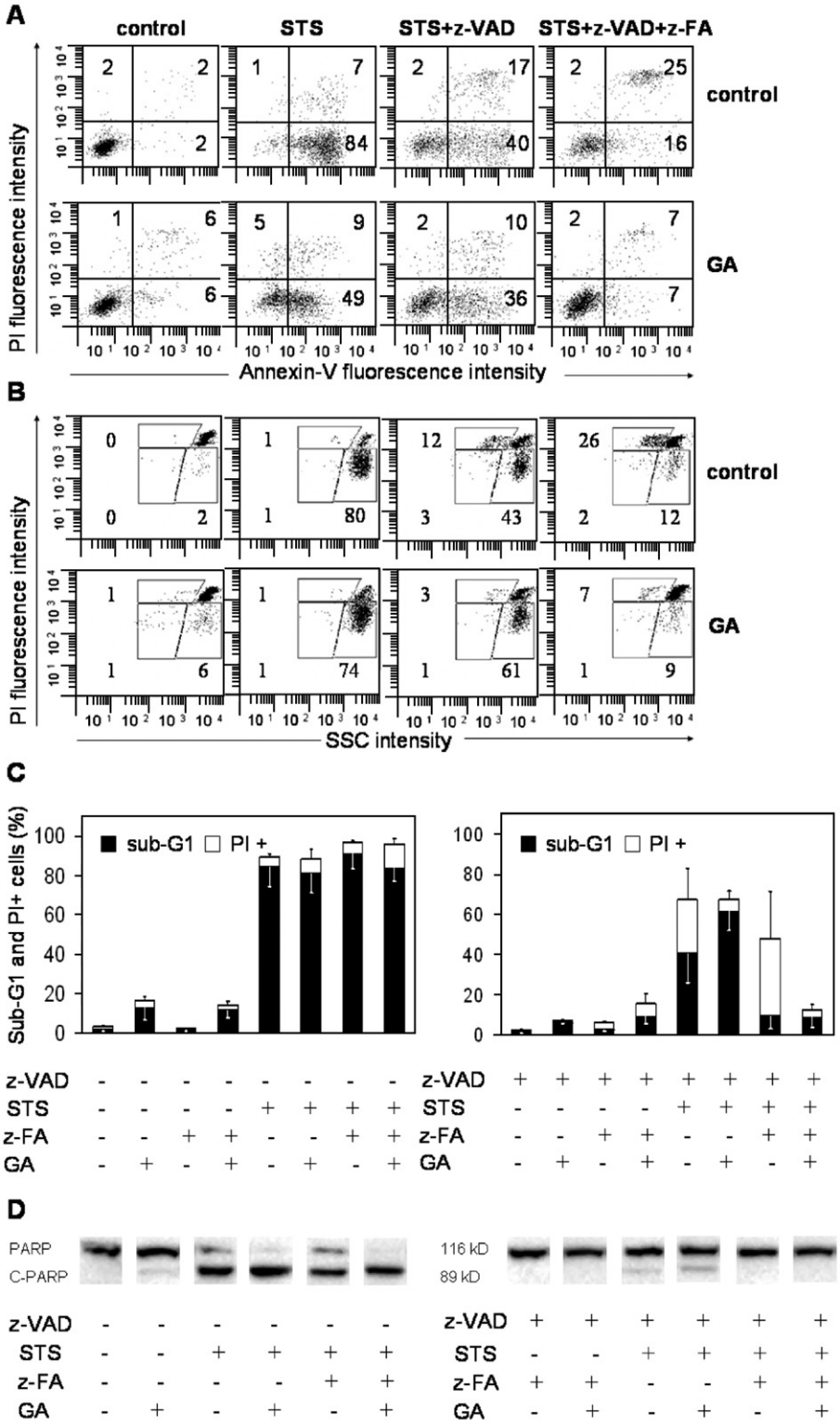

Fig. 4. Regulation of the appearance of cell death forms induced by staurosporine. (A–D) U937 cells were exposed to STS (1 μM) in the presence or absence of z-VAD.fmk (50 μM) for 8 h. Samples were preincubated with or without GA (1 μM) for 12 h and/or z-FA.fmk (z-FA) (1 μM) for 30 min. (A) Representative histograms of annexin V-FITC and PI stained, unfixed samples detected by flow cytometry and evaluated in [Annexin V-FITC, PI] representation. (B) Representative histograms of PI-stained, ethanol fixed samples detected by flow cytometry and evaluated in [SSC, DNA content] representation. The values indicate the percentage of cells in marked regions. DMSO as vehicle was applied for control samples. (C) Column diagrams of data quantified in [sub-G1] and [PI uptake] flow cytometric representations. Values are mean±SD ($n=5$). (D) Western blot analysis. PARP: full length PARP (116 kDa), C-PARP: cleaved PARP fragment (89 kDa).

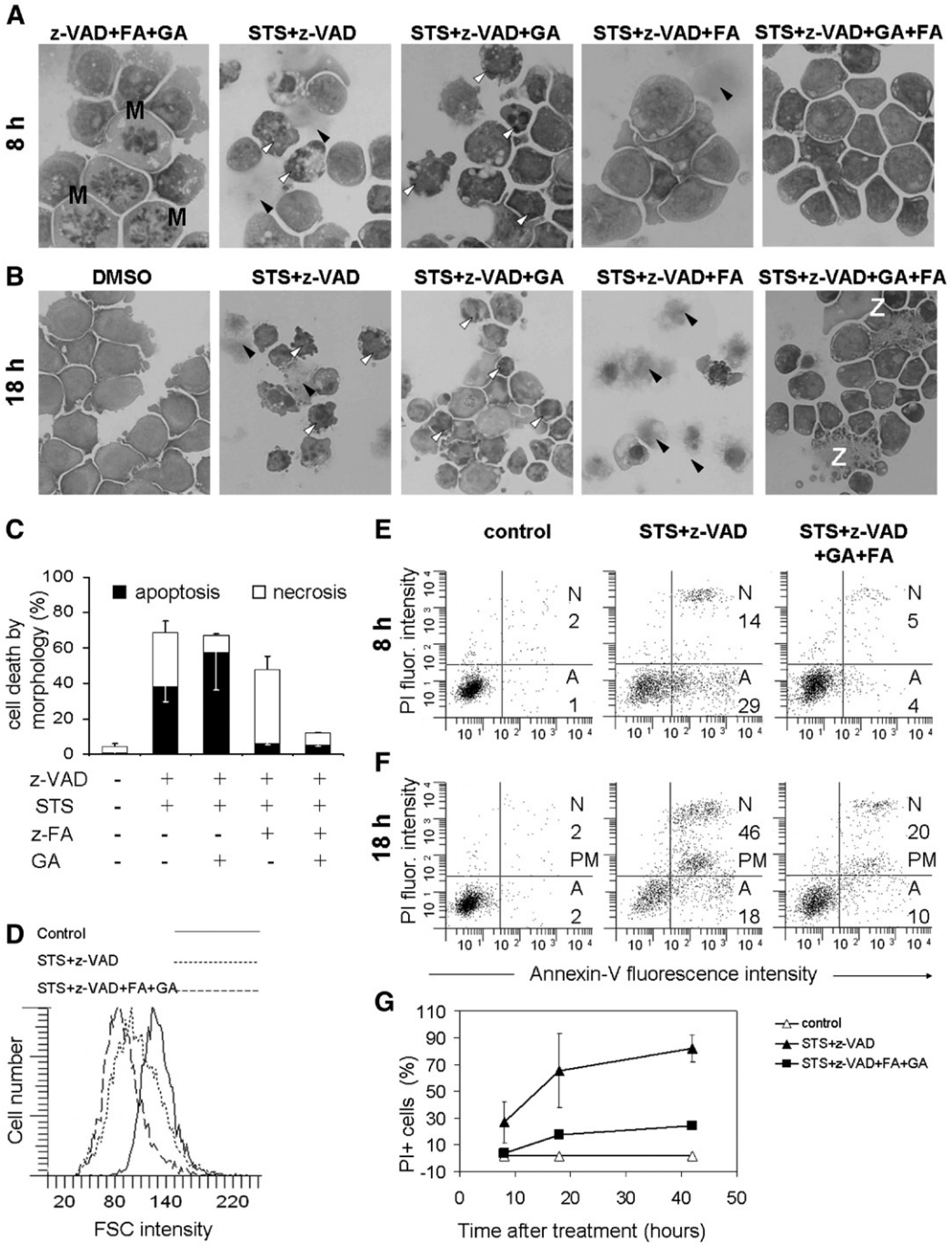

Fig. 5. GA+z-FA.fmk protected caspase-compromised cells from STS-induced cell death for prolonged time. (A–F) U937 cells were exposed to STS (1 μM) in the presence or absence of z-VAD.fmk (50 μM) for 8 h. Samples were preincubated with or without GA (1 μM) for 12 h and/or z-FA.fmk (z-FA, FA) (1 μM) for 30 min. Treated samples were harvested for light microscopic analysis at (A) 8 h and (B) 18 h. Black arrow: necrotic cells, white arrow: apoptotic cells, Z: zeiotic cells, M: Mitotic cells. (C) Cell death was quantified as apoptosis and necrosis by light microscopic morphological analysis. Values are mean±SD (n=2). (D) Treated samples were prepared according to [PI uptake] flow cytometric representation and the FSC (forward light scatter) intensity of PI unstained, vital cells was presented. DMSO as vehicle (continuos line), STS+z-VAD (dotted line), STS+z-VAD+GA+FA (dashed line) (representative of n=5). (E, F) Representative histograms of annexin V-FITC and PI-stained, unfixed samples detected by flow cytometry and evaluated in [Annexin V-FITC, PI] representation (E) 8 h and (F) 18 h after treatment. N: necrotic cells, PM: post mortem cells, A: apoptotic cells. Values are indicate the percentage of cells in the quadrate regions (n=2). (G) Diagram shows long-term kinetics of absolute percentage of PI+ cells measured with Flow cytometry in [PI uptake] flow cytometric representation (n=2). Samples were treated with DMSO as vehicle (open triangle), STS+z-VAD (black triangle), STS+z-VAD+GA+FA (black square).

SSC decrease) were reduced by co-treatment with the two inhibitors (Fig. 4A, B) after 8 h of treatment. The abrogation of cell death (both apoptotic and necrotic) was significant in the [sub-G1—PI-uptake] profile (P<0.00002) (Fig. 4C) and the [SSC—DNA content] profile (not shown). GA+z-FA.fmk had no significant effect on apoptosis induced by STS (Fig. 4C) or on necrosis induced by H_2O_2 (not shown), underlining the diversity in death pathways. Co-treated cells preserved the

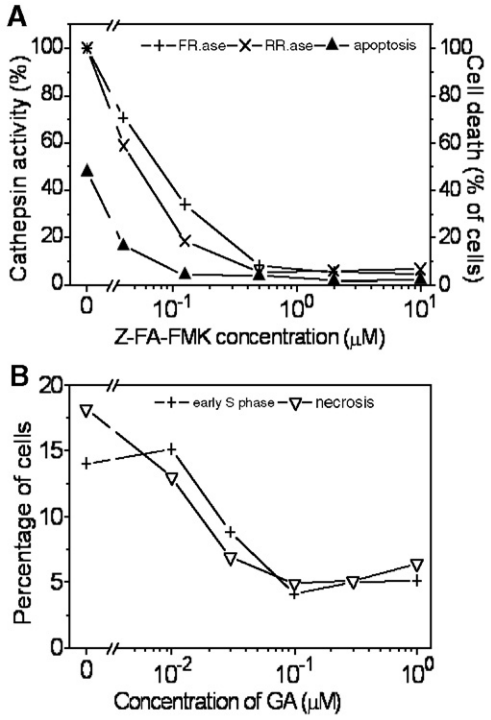

Fig. 6. Correlation of the effect of z-FA.fmk and GA on different cell functions. U937 cells were pre-incubated with various dilutions of (A): z-FA.fmk for 30 min or (B): geldanamycin for 12 h, then exposed to DMSO as control or STS+z-VAD.fmk for 8 h. (A) Cathepsin activity were detected in samples treated with z-FA.fmk dilutions by z-FR-AMC (–+–) and z-RR-AMC (–x–) fluorogenic substrates and the slope of the linear activity values were plotted as percentage compared to control (no z-FA.fmk added) sample. Apoptosis was determined in the [sub-G1] flow cytometric representation (filled up triangles), and absolute percentage of these cells were plotted. (B) Cell cycle distribution was determined by flow cytometry and absolute percentage of cells of early S phase was plotted (–x–). Necrosis was evaluated in the [PI uptake] flow cytometric representation and absolute percentage of these cells was plotted (open down triangles). Representative of two independent experiments is presented.

cytoplasmic and nuclear structures but had reduced volume compared to control cells (Fig. 5A, B). The flow cytometric forward (light) scatter (FSC) value is usually proportional to the volume of viable cells. Detection of the FSC parameter confirmed that GA+z-FA.fmk could not protect STS+z-VAD.fmk-generated cell volume loss (Fig. 5D). Nevertheless, the viability of STS+z-VAD.fmk-exposed cells was preserved for a long time with GA+z-FA.fmk, at least partially, which was assessed by morphology (Fig. 5A, B), [annexin V—PI] (Fig. 5 E, F) and [PI uptake] (Fig. 5G) flow cytometric death profiles. As volume loss is an upstream phenomenon in cell death, we tested whether the mitochondria and/or lysosomal functions were preserved with GA+z-FA.fmk. We assessed mitochondrial membrane potential with $DiOC_6(3)$ staining (Fig. 7A, B) and the extent of acidic (endo-lysosomal) compartments with acridine orange (AO) (Fig. 7E, F) using flow cytometry. STS alone induced a moderate decrease of both mitochondrial membrane potential and volume of acidic compartments. STS+z-VAD.fmk reduced both stainings even more (Fig. 7A, E). However, z-FA.fmk and GA combination prevented the reduction of both stainings induced by STS+z-VAD.fmk, but not in the case when z-VAD.fmk was omitted from STS (Fig. 7B, F). A representation of mean fluorescence intensities shows that GA+z-FA.fmk significantly preserved both the mitochondrial membrane potential and the volume of acidic compartments in U937 cells exposed to STS+z-VAD.fmk (Fig. 7D and H) but not in cells exposed to STS (Fig. 7C and G) or H_2O_2 (data not shown).

4. Discussion

In this study we used STS as a model compound for induction of cell death via the intrinsic mitochondria-apoptosome mediated pathway. We have shown that STS, in the presence of z-VAD.fmk caspase inhibitor, evoked apoptotic as well as necrotic forms of cell death in parallel in distinct cells but not the mixed phenotype in individual cells. For assessment apoptotic and necrotic traits in individual cells we introduced a new flow cytometric death profile by correlating SSC and DNA content changes in ethanol fixed cells. This technique allowed us to complement the usual dye uptake assay for detection of necrosis. The two methods using them in parallel may allow one to discriminate between primary necrotic and secondary necrotic cell exploiting that primary necrotic cells usually do not bear immediate small scale DNA fragmentation while secondary necrotic cell do. Furthermore, primary necrotic cells arising in case of caspase inhibition loss their SSC value rapidly, while secondary necrotic cells only gradually (Fig. 2D, STS 20 h). However, post-mortem changes in dead cells might deteriorate these differences due to serum DNases and proteases as demonstrated in Fig. 5E, F.

Using this and other flow cytometric death profiles complemented with morphological investigation and PARP processing test we found that both z-FA.fmk, the inhibitor of cystein proteases and GA, the inhibitor of Hsp90 chaperone activity switched one of the cell death form to the other in STS-induced caspase-compromised U937 cells. Furthermore, z-FA.fmk and GA combination halted cell death by preserving mitochondrial membrane potential and the acidic volume of cells (Fig. 7) while not preventing cell shrinkage (Fig. 5).

Searching for biochemical markers typical for apoptosis or necrosis in this experimental circumstances we found that the applied dose of z-VAD.fmk completely suppressed the activity of the so-called executioner caspases (DEVDases) induced by STS. Nevertheless, nucleosomal DNA fragmentation, PARP cleavage typical in caspase-mediated apoptosis [35] and morphological condensation of DNA was not abrogated by z-VAD.fmk, those were only initiated with a delayed kinetics. Application of z-FA.fmk abolished all the three detected features of apoptosis. This indicates a role for cystein proteases in mediating the apoptotic signal provoked by STS in caspase-compromised U937 cells. The more precise characterization of this cystein protease as cathepsins comes from the results that (a) z-VAD.fmk exposed cells retained a fractional FRase activity, featuring a broader range of cystein cathepsins, while lost RRase activity, that specify cathepsin B primarily [37]; (b) z-FA.fmk inhibited both apoptosis and FRase activity in cells at the same concentrations.

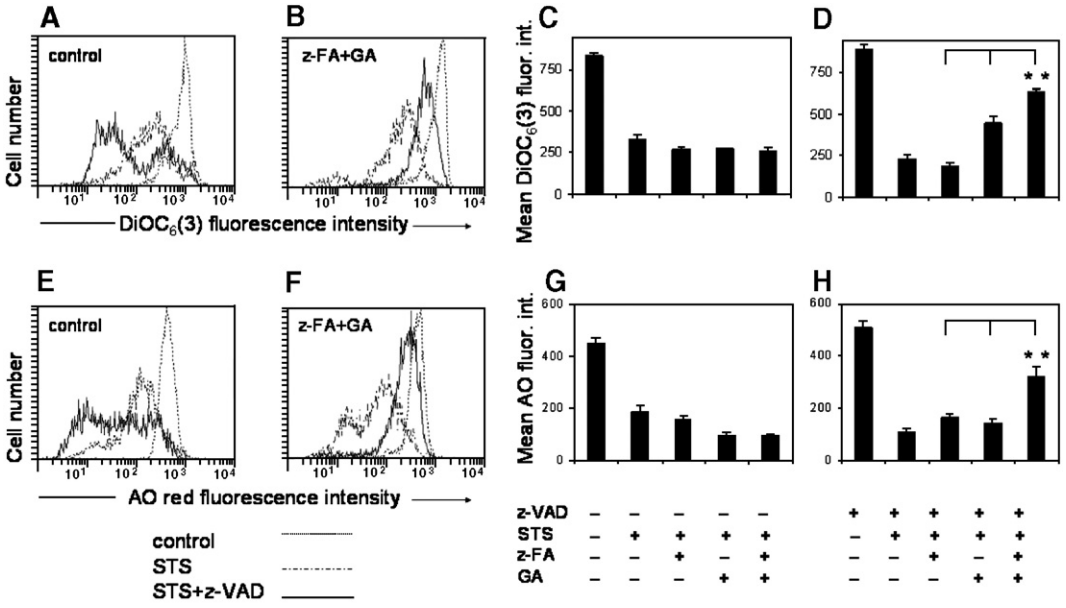

Fig. 7. Protection of cells from staurosporine-induced cell death was accompanied with prevention of mitochondrial and lysosomal breakdown. U937 cells were exposed to STS (1 μM) in the presence or absence of z-VAD.fmk (50 μM) for 8 h. Samples were preincubated with or without GA (1 μM) for 12 h and/or z-FA.fmk (1 μM) for 30 min. (A–B) Representative histograms of $DiOC_6(3)$ and PI-stained samples detected by flow cytometry and presented in [$DiOC_6(3)$] representation. (E–F) Representative histograms of AO-stained samples detected by flow cytometry and presented in [AO red] representation. Samples were treated with (A, E) DMSO as control or with (B, F) GA + z-FA.fmk together with DMSO as control (dotted lines), STS (dashed lines) or STS + z-VAD.fmk (continuos lines). (C–D) Column diagrams of data quantified in [$DiOC_6(3)$] flow cytometric representation as mean fluorescence intensity of the whole gated cell population. (G–H) Column diagrams of data quantified in [AO red] flow cytometric representation as mean fluorescence intensity of the whole gated cell population. Values are mean ± SD (n = 3).

Others have shown previously that U937 express at least cathepsin B, -H, -L, -S cystein cathepsins at moderate while cathepsin D at excess level [23,30]. However, an activity-based probe for cystein cathepsin visualized other bands in endocytic fraction. It is not clear that these proteases can directly access and process the appropriate substrate proteins required for apoptotic transformation as do effector caspases [28]. Purified cathepsins could not directly activate caspases [47], but isolated lysosomes have done [27]. Purified cathepsin B and L could processed cPLA2 [17], purified cathepsin B, -D and -G cleaved PARP [20] but providing fragments with different lengths compared to caspases. However, again isolated lysosomes could yield the typical apoptotic fragment length of PARP [20] or the Bid fragment that functionally identical with the caspase-processed one [47]. Interestingly, Brockhaus and Brüne found in U937 cells that NO-releasing compounds induced DNA fragmentation and U1 snRNP cleavage (at 4 h treatment) that were abrogated by using a pan caspase inhibitor, but the typical apoptotic fragment length of PARP (85 kDa) appeared with delayed kinetics (after 8 h treatment) [5]. But there is no information about the role of cathepsins in this phenomenon.

Indirect evidences indicate that TNF-α in hepatocytes [59] or bortezomib in pancreatic cancer cells [61] stimulated the release of cathepsin (B) from lysosomes that was required for caspase 2 activation and mitochondrial permeabilization providing the source of caspase-dependent and -independent effector molecules of apoptosis, including AIF [12] and endonuclease G [34]. Caspase 2 is less sensitive for z-VAD.fmk than other caspases [19], therefore it is possible that caspase 2 can serve as a proteolytic dart for cathepsins. PIDDosome forms a platform for activation of caspase 2 [53] and RIP1 as well [29]. Autoproteolysis of PIDD at two different sites provides fragments for preferable caspase 2 or RIP1 activation [52]. It is an intriguing hypothesis that the PIDDosome can realize the suggested bifurcation point where cathepsin mediated proteolysis set up the decision making point of cells to commit apoptotic or necrotic suicide when executioner caspases are halted by drugs or IAP proteins. This and other [40] possible involvements of caspase activities in the execution of cell death without DEVDase activity forced us to consistently apply the terminology as caspase-compromised or caspase-inhibited instead of caspase-independent for z-VAD.fmk-treated cells in this study.

The permeabilization of lysosomes may serve for another putative bifurcation point. It is proposed that low grade leakage of lysosomes preferably initiates apoptotic signaling, while high grade disruption of lysosomes favorably promotes necrosis [7]. Permeabilization is advanced by excess oxidation of lipids and proteins [51] while Hsp 70 expression favors stabilization of the lysosomes probably assisting the selective permeability of their membrane [39]. Abruption of Hsp90 function by GA provokes Hsp70 upregulation that may preserve lysosomes and suppress necrosis. However this scenario is unlikely because GA pretreatment could not prevent STS+z-VAD.fmk-generated decline of AO red staining (Fig. 7H) indicating of lysosomal damage, at least abruption of H^+ homeostasis. Interestingly, mitochondrial depolarization was partially prevented by prolonged exposure of U937 cell to GA (Fig. 7D). Another difficulty of this hypothesis comes up with considering how disruption of the activity of cathepsins by z-FA.fmk will assist for necrosis instead of apoptosis.

Nevertheless, our results are consistent with the interpretation of the existence of a bifurcation point in the STS-induced death signal pathway positioned at or upstream of mitochondrial and lysosomal breakdown. This pathway may dominate in cells where executioner caspases are suppressed. Caspase-compromised states can occur in physiological and pathological circumstances by over-expression of inhibitor of apoptosis proteins (IAPs) [13], over-production of nitric oxide (NO) that may nitrosylates and inactivates caspases [6,41], or application of drugs that result in reactive metabolite formation and oxidative stress e.g. the case of acetaminophen [24]. The use of caspase inhibitors can partially mimic these patho-physiological cases. Furthermore, consideration of caspase inhibitors (even with broader specificity) as potential pharmaceutical products requires exploration of the molecular mechanisms of "caspase-independent cell death.

Acknowledgments

We thank Sandor Paku (Semmelweis University, Budapest) for excellent advices and technical assistance on electron microscopy, Pal Bauer, Katalin Nagy and Melinda Hajdu (Semmelweis University, Budapest) for technical help on western blot, Laszlo Kopper, Anna Sebestyen, and Katalin Nagy (Semmelweis University, Budapest) for discussions, Janos Matko (Eotvos L Univ., Budapest) for critically reading the manuscript.

R.M. was supported by grants from the Hungarian Scientific Research grant (OTKA T 049008). I. P. was supported by NKFP IA/002/2004, OTKA-T046665, OMFB-00287/2005, Szentágothai János Knowledge and supported by National Office for Research and Technology (NKTH), Hungary.

References

[1] G.P. Amarante-Mendes, D.M. Finucane, S.J. Martin, T.G. Cotter, G.S. Salvesen, D.R. Green, Anti-apoptotic oncogenes prevent caspase-dependent and independent commitment for cell death, Cell Death Differ. 5 (1998) 298–306.

[2] K. Andreau, M. Castedo, J.L. Perfettini, T. Roumier, E. Pichart, S. Souquere, S. Vivet, N. Larochette, G. Kroemer, Preapoptotic chromatin condensation upstream of the mitochondrial checkpoint, J. Biol. Chem. 279 (2004) 55937–55945.

[3] M. Bedin, A.M. Gaben, C. Saucier, J. Mester, Geldanamycin, an inhibitor of the chaperone activity of HSP90, induces MAPK-independent cell cycle arrest, Int. J. Cancer 109 (2004) 643–652.

[4] C.A. Belmokhtar, J. Hillion, C. Dudognon, S. Fiorentino, M. Flexor, M. Lanotte, E. Segal-Bendirdjian, Apoptosome-independent pathway for apoptosis. Biochemical analysis of APAF-1 defects and biological outcomes, J. Biol. Chem. 278 (2003) 29571–29580.

[5] F. Brockhaus, B. Brune, U937 apoptotic cell death by nitric oxide: Bcl-2 downregulation and caspase activation, Exp. Cell Res. 238 (1998) 33–41.

[6] B. Brune, Nitric oxide: NO apoptosis or turning it ON? Cell Death Differ. 10 (2003) 864–869.

[7] U.T. Brunk, H. Dalen, K. Roberg, H.B. Hellquist, Photo-oxidative disruption of lysosomal membranes causes apoptosis of cultured human fibroblasts, Free Radic. Biol. Med. 23 (1997) 616–626.

[8] M. Capano, M. Crompton, Biphasic translocation of Bax to mitochondria, Biochem. J. 367 (2002) 169–178.

[9] B.S. Cummings, G.R. Kinsey, L.J. Bolchoz, R.G. Schnellmann, Identification of caspase-independent apoptosis in epithelial and cancer cells, J. Pharmacol. Exp. Ther. 310 (2004) 126–134.

[10] Z. Darzynkiewicz, E. Bedner, Analysis of apoptotic cells by flow and laser scanning cytometry, Methods Enzymol. 322 (2000) 18–39.

[11] Z. Darzynkiewicz, G. Juan, X. Li, W. Gorczyca, T. Murakami, F. Traganos, Cytometry in cell necrobiology: analysis of apoptosis and accidental cell death (necrosis), Cytometry 27 (1997) 1–20.

[12] E. Daugas, S.A. Susin, N. Zamzami, K.F. Ferri, T. Irinopoulou, N. Larochette, M.C. Prevost, B. Leber, D. Andrews, J. Penninger, G. Kroemer, Mitochondrio-nuclear translocation of AIF in apoptosis and necrosis, FASEB J. 14 (2000) 729–739.

[13] A.O. de Graaf, T. de Witte, J.H. Jansen, Inhibitor of apoptosis proteins: new therapeutic targets in hematological cancer? Leukemia 18 (2004) 1751–1759.

[14] O. Deas, C. Dumont, M. MacFarlane, M. Rouleau, C. Hebib, F. Harper, F. Hirsch, B. Charpentier, G.M. Cohen, A. Senik, Caspase-independent cell death induced by anti-CD2 or staurosporine in activated human peripheral T lymphocytes, J. Immunol. 161 (1998) 3375–3383.

[15] C. Ferraro-Peyret, L. Quemeneur, M. Flacher, J.P. Revillard, L. Genestier, Caspase-independent phosphatidylserine exposure during apoptosis of primary T lymphocytes, J. Immunol. 169 (2002) 4805–4810.

[16] N. Festjens, T. Vanden Berghe, P. Vandenabeele, Necrosis, a well-orchestrated form of cell demise: signalling cascades, important mediators and concomitant immune response, Biochim. Biophys. Acta 1757 (2006) 1371–1387.

[17] L. Foghsgaard, U. Lademann, D. Wissing, B. Poulsen, M. Jaattela, Cathepsin B mediates tumor necrosis factor-induced arachidonic acid release in tumor cells, J. Biol. Chem. 277 (2002) 39499–39506.

[18] L. Foghsgaard, D. Wissing, D. Mauch, U. Lademann, L. Bastholm, M. Boes, F. Elling, M. Leist, M. Jaattela, Cathepsin B acts as a dominant execution protease in tumor cell apoptosis induced by tumor necrosis factor, J. Cell Biol. 153 (2001) 999–1010.

[19] M. Garcia-Calvo, E.P. Peterson, B. Leiting, R. Ruel, D.W. Nicholson, N.A. Thornberry, Inhibition of human caspases by peptide-based and macromolecular inhibitors, J. Biol. Chem. 273 (1998) 32608–32613.

[20] S. Gobeil, C.C. Boucher, D. Nadeau, G.G. Poirier, Characterization of the necrotic cleavage of poly(ADP-ribose) polymerase (PARP-1): implication of lysosomal proteases, Cell Death Differ. 8 (2001) 588–594.

[21] P. Golstein, G. Kroemer, Cell death by necrosis: towards a molecular definition, Trends Biochem. Sci. 32 (2007) 37–43.

[22] J. Gong, F. Traganos, Z. Darzynkiewicz, A selective procedure for DNA extraction from apoptotic cells applicable for gel electrophoresis and flow cytometry, Anal. Biochem. 218 (1994) 314–319.

[23] A. Greiner, A. Lautwein, H.S. Overkleeft, E. Weber, C. Driessen, Activity and subcellular distribution of cathepsins in primary human monocytes, J. Leukoc. Biol. 73 (2003) 235–242.

[24] J.S. Gujral, T.R. Knight, A. Farhood, M.L. Bajt, H. Jaeschke, Mode of cell death after acetaminophen overdose in mice: apoptosis or oncotic necrosis? Toxicol. Sci. 67 (2002) 322–328.

[25] C.A. Hetz, M. Hunn, P. Rojas, V. Torres, L. Leyton, A.F. Quest, Caspase-dependent initiation of apoptosis and necrosis by the Fas receptor in lymphoid cells: onset of necrosis is associated with delayed ceramide increase, J. Cell Sci. 115 (2002) 4671–4683.

[26] N. Holler, R. Zaru, O. Micheau, M. Thome, A. Attinger, S. Valitutti, J.L. Bodmer, P. Schneider, B. Seed, J. Tschopp, Fas triggers an alternative, caspase-8-independent cell death pathway using the kinase RIP as effector molecule, Nat. Immunol. 1 (2000) 489–495.

[27] R. Ishisaka, T. Utsumi, M. Yabuki, T. Kanno, T. Furuno, M. Inoue, K. Utsumi, Activation of caspase-3-like protease by digitonin-treated lysosomes, FEBS Lett. 435 (1998) 233–236.

[28] M. Jaattela, J. Tschopp, Caspase-independent cell death in T lymphocytes, Nat. Immunol. 4 (2003) 416–423.

[29] S. Janssens, A. Tinel, S. Lippens, J. Tschopp, PIDD mediates NF-kappaB activation in response to DNA damage, Cell 123 (2005) 1079–1092.

[30] A. Journet, A. Chapel, S. Kieffer, F. Roux, J. Garin, Proteomic analysis of human lysosomes: application to monocytic and breast cancer cells, Proteomics 2 (2002) 1026–1040.

[31] M. Kalai, G. Van Loo, T. Vanden Berghe, A. Meeus, W. Burm, X. Saelens, P. Vandenabeele, Tipping the balance between necrosis and apoptosis in human and murine cells treated with interferon and dsRNA, Cell Death Differ. 9 (2002) 981–994.

[32] M. Leist, M. Jaattela, Four deaths and a funeral: from caspases to alternative mechanisms, Nat. Rev., Mol. Cell Biol. 2 (2001) 589–598.
[33] M. Leist, B. Single, A.F. Castoldi, S. Kuhnle, P. Nicotera, Intracellular adenosine triphosphate (ATP) concentration: a switch in the decision between apoptosis and necrosis, J. Exp. Med. 185 (1997) 1481–1486.
[34] L.Y. Li, X. Luo, X. Wang, Endonuclease G is an apoptotic DNase when released from mitochondria, Nature 412 (2001) 95–99.
[35] X. Li, Z. Darzynkiewicz, Cleavage of Poly(ADP-ribose) polymerase measured in situ in individual cells: relationship to DNA fragmentation and cell cycle position during apoptosis, Exp. Cell Res. 255 (2000) 125–132.
[36] R. Mihalik, G. Imre, I. Petak, B. Szende, L. Kopper, Cathepsin B-independent abrogation of cell death by CA-074-OMe upstream of lysosomal breakdown, Cell Death Differ. 11 (2004) 1357–1360.
[37] I. Mlinaric-Rascan, B. Turk, B cell receptor-mediated nuclear fragmentation proceeds in WEHI 231 cells in the absence of detectable DEVDase and FRase activity, FEBS Lett. 553 (2003) 51–55.
[38] P. Nicotera, G. Melino, Regulation of the apoptosis-necrosis switch, Oncogene 23 (2004) 2757–2765.
[39] J. Nylandsted, M. Gyrd-Hansen, A. Danielewicz, N. Fehrenbacher, U. Lademann, M. Hoyer-Hansen, E. Weber, G. Multhoff, M. Rohde, M. Jaattela, Heat shock protein 70 promotes cell survival by inhibiting lysosomal membrane permeabilization, J. Exp. Med. 200 (2004) 425–435.
[40] C. Rebe, S. Cathelin, S. Launay, R. Filomenko, L. Prevotat, C. L'Ollivier, E. Gyan, O. Micheau, S. Grant, A. Dubart-Kupperschmitt, M. Fontenay, E. Solary, Caspase-8 prevents sustained activation of NF-kappaB in monocytes undergoing macrophagic differentiation, Blood 109 (2007) 1442–1450.
[41] L. Rossig, B. Fichtlscherer, K. Breitschopf, J. Haendeler, A.M. Zeiher, A. Mulsch, S. Dimmeler, Nitric oxide inhibits caspase-3 by S-nitrosation in vivo, J. Biol. Chem. 274 (1999) 6823–6826.
[42] J. Rozman-Pungercar, N. Kopitar-Jerala, M. Bogyo, D. Turk, O. Vasiljeva, I. Stefe, P. Vandenabeele, D. Bromme, V. Puizdar, M. Fonovic, M. Trstenjak-Prebanda, I. Dolenc, V. Turk, B. Turk, Inhibition of papain-like cysteine proteases and legumain by caspase-specific inhibitors: when reaction mechanism is more important than specificity, Cell Death Differ. 10 (2003) 881–888.
[43] J.L. Scarlett, P.W. Sheard, G. Hughes, E.C. Ledgerwood, H.H. Ku, M.P. Murphy, Changes in mitochondrial membrane potential during staurosporine-induced apoptosis in Jurkat cells, FEBS Lett. 475 (2000) 267–272.
[44] P. Schotte, W. Declercq, S. Van Huffel, P. Vandenabeele, R. Beyaert, Non-specific effects of methyl ketone peptide inhibitors of caspases, FEBS Lett. 442 (1999) 117–121.
[45] S.L. Springs, V.M. Diavolitsis, J. Goodhouse, G.L. McLendon, The kinetics of translocation of Smac/DIABLO from the mitochondria to the cytosol in HeLa cells, J. Biol. Chem. 277 (2002) 45715–45718.
[46] C.E. Stebbins, A.A. Russo, C. Schneider, N. Rosen, F.U. Hartl, N.P. Pavletich, Crystal structure of an Hsp90–geldanamycin complex: targeting of a protein chaperone by an antitumor agent, Cell 89 (1997) 239–250.
[47] V. Stoka, B. Turk, S.L. Schendel, T.H. Kim, T. Cirman, S.J. Snipas, L.M. Ellerby, D. Bredesen, H. Freeze, M. Abrahamson, D. Bromme, S. Krajewski, J.C. Reed, X.M. Yin, V. Turk, G.S. Salvesen, Lysosomal protease pathways to apoptosis. Cleavage of bid, not pro-caspases, is the most likely route, J. Biol. Chem. 276 (2001) 3149–3157.
[48] M. Tafani, J.A. Cohn, N.O. Karpinich, R.J. Rothman, M.A. Russo, J.L. Farber, Regulation of intracellular pH mediates Bax activation in HeLa cells treated with staurosporine or tumor necrosis factor-alpha, J. Biol. Chem. 277 (2002) 49569–49576.
[49] M. Tafani, D.A. Minchenko, A. Serroni, J.L. Farber, Induction of the mitochondrial permeability transition mediates the killing of HeLa cells by staurosporine, Cancer Res. 61 (2001) 2459–2466.
[50] T. Tamaoki, H. Nomoto, I. Takahashi, Y. Kato, M. Morimoto, F. Tomita, Staurosporine, a potent inhibitor of phospholipid/Ca++ dependent protein kinase, Biochem. Biophys. Res. Commun. 135 (1986) 397–402.
[51] A. Terman, T. Kurz, B. Gustafsson, U.T. Brunk, Lysosomal labilization, IUBMB Life 58 (2006) 531–539.
[52] A. Tinel, S. Janssens, S. Lippens, S. Cuenin, E. Logette, B. Jaccard, M. Quadroni, J. Tschopp, Autoproteolysis of PIDD marks the bifurcation between pro-death caspase-2 and pro-survival NF-kappaB pathway, EMBO J. 26 (2007) 197–208.
[53] A. Tinel, J. Tschopp, The PIDDosome, a protein complex implicated in activation of caspase-2 in response to genotoxic stress, Science 304 (2004) 843–846.
[54] F. Traganos, Z. Darzynkiewicz, Lysosomal proton pump activity: supravital cell staining with acridine orange differentiates leukocyte subpopulations, Methods Cell Biol. 41 (1994) 185–194.
[55] K. van Leyen, A. Siddiq, R.R. Ratan, E.H. Lo, Proteasome inhibition protects HT22 neuronal cells from oxidative glutamate toxicity, J. Neurochem. 92 (2005) 824–830.
[56] T. Vanden Berghe, G. van Loo, X. Saelens, M. Van Gurp, G. Brouckaert, M. Kalai, W. Declercq, P. Vandenabeele, Differential signaling to apoptotic and necrotic cell death by Fas-associated death domain protein FADD, J. Biol. Chem. 279 (2004) 7925–7933.
[57] D. Vercammen, G. Brouckaert, G. Denecker, M. Van de Craen, W. Declercq, W. Fiers, P. Vandenabeele, Dual signaling of the Fas receptor: initiation of both apoptotic and necrotic cell death pathways, J. Exp. Med. 188 (1998) 919–930.
[58] M.C. Wei, W.X. Zong, E.H. Cheng, T. Lindsten, V. Panoutsakopoulou, A.J. Ross, K.A. Roth, G.R. MacGregor, C.B. Thompson, S.J. Korsmeyer, Proapoptotic BAX and BAK: a requisite gateway to mitochondrial dysfunction and death, Science 292 (2001) 727–730.
[59] N.W. Werneburg, M.E. Guicciardi, S.F. Bronk, G.J. Gores, Tumor necrosis factor-alpha-associated lysosomal permeabilization is cathepsin B dependent, Am. J. Physiol. Gasterointest. Liver Physiol. 283 (2002) G947–G956.
[60] K.T. Yang, W.L. Chang, P.C. Yang, C.L. Chien, M.S. Lai, M.J. Su, M.L. Wu, Activation of the transient receptor potential M2 channel and poly (ADP-ribose) polymerase is involved in oxidative stress-induced cardiomyocyte death, Cell Death Differ. 13 (2006) 1815–1826.
[61] B.H. Yeung, D.C. Huang, F.A. Sinicrope, PS-341 (bortezomib) induces lysosomal cathepsin B release and a caspase-2-dependent mitochondrial permeabilization and apoptosis in human pancreatic cancer cells, J. Biol. Chem. 281 (2006) 11923–11932.
[62] X.D. Zhang, S.K. Gillespie, P. Hersey, Staurosporine induces apoptosis of melanoma by both caspase-dependent and -independent apoptotic pathways, Mol. Cancer Ther. 3 (2004) 187–197.
[63] P. Zhou, L. Qian, C. Iadecola, Nitric oxide inhibits caspase activation and apoptotic morphology but does not rescue neuronal death, J. Cereb. Blood Flow Metab. 25 (2005) 348–357.
[64] W.X. Zong, T. Lindsten, A.J. Ross, G.R. MacGregor, C.B. Thompson, BH3-only proteins that bind pro-survival Bcl-2 family members fail to induce apoptosis in the absence of Bax and Bak, Genes Dev. 15 (2001) 1481–1486.
[65] H. Zou, Y. Li, X. Liu, X. Wang, An APAF-1.cytochrome *c* multimeric complex is a functional apoptosome that activates procaspase-9, J. Biol. Chem. 274 (1999) 11549–11556.